

NEAR INFRARED FAINT GALAXIES IN THE SUBARU DEEP FIELD: COMPARING THE THEORY WITH OBSERVATIONS FOR GALAXY COUNTS, COLORS, AND SIZE DISTRIBUTIONS TO  $K \sim 24.5^*$ 

TOMONORI TOTANI

Theory Division, National Astronomical Observatory, Mitaka, Tokyo 181-8588, Japan

(E-mail: totani@th.nao.ac.jp)

(present address: Princeton University Observatory, Peyton Hall, Princeton, NJ 08544, USA)

YUZURU YOSHII<sup>†</sup>

Institute of Astronomy, School of Science, The University of Tokyo, Mitaka, Tokyo 181-8588, Japan

TOSHINORI MAIHARA

Department of Astronomy, Kyoto University, Kitashirakawa, Kyoto 606-8502, Japan

FUMIHIDE IWAMURO

Department of Physics, Kyoto University, Kitashirakawa, Kyoto 606-8502, Japan

AND

KENTARO MOTOHARA

Subaru Telescope, National Astronomical Observatory of Japan, 650 North A'ohoku Place, Hilo, HI 96720, USA

*To Appear in the Astrophysical Journal*

## ABSTRACT

Galaxy counts in the  $K$  band,  $(J-K)$ -colors, and apparent size distributions of faint galaxies in the Subaru Deep Field (SDF) down to  $K \sim 24.5$  were studied in detail. Special attention has been paid to take into account various selection effects including the cosmological dimming of surface brightness, to avoid any systematic bias which may be the origin of controversy in previously published results. We also tried to be very careful about systematic model uncertainties; we present a comprehensive surveys of these systematic uncertainties and dependence on various parameters, and we have shown that the dominant factors to determine galaxy counts in this band are cosmology and number evolution. We found that the pure luminosity evolution (PLE) model is well consistent with all the SDF data down to  $K \sim 22.5$ , without any evidence for number or size evolution in a low-density,  $\Lambda$ -dominated flat universe which is now favored by various cosmological observations. On the other hand, a number evolution of galaxies with  $\eta \sim 2$ , when invoked as the luminosity conserving mergers as  $\phi^* \propto (1+z)^\eta$  and  $L^* \propto (1+z)^{-\eta}$  for all types of galaxies, is necessary to explain the data in the Einstein-de Sitter universe. If the popular  $\Lambda$ -dominated universe is taken for granted, our result then gives a strong constraint on the number evolution of giant elliptical or early-type galaxies to  $z \sim 1-2$  which must be met by any models in the hierarchically clustering universe, since such galaxies are the dominant population in this magnitude range ( $K \lesssim 22.5$ ). A number evolution with  $\eta \sim 1$  is already difficult to reconcile with the data in this universe. On the other hand number evolution of late type galaxies and/or dwarf galaxies, which has been suggested by previous studies of optical galaxies, is allowed from the data. In the fainter magnitude range of  $K \gtrsim 22.5$ , we found a slight excess of observed counts over the prediction of the PLE model when elliptical galaxies are treated as a single population. We suggest that this discrepancy reflects some number evolution of dwarf galaxies and/or the distinct populations of giant and dwarf elliptical galaxies which have been known for local elliptical galaxies.

*Subject headings:* cosmology: observations — galaxies: evolution — galaxies: formation

\*Based on the data corrected at the Subaru telescope, which is operated by the National Astronomical Observatory of Japan.

<sup>†</sup>Also Research Center for the Early Universe, Faculty of Science, The University of Tokyo, Tokyo 113-0033, Japan.

## 1. INTRODUCTION

Deep surveys in the extragalactic universe give the most fundamental information to understand when and how galaxies formed and evolved, as well as the large-scale structure and geometry of our universe. The best image in the optical wavelengths has been obtained by the Hubble Space Telescope (Williams et al. 1996; Williams et al. 2000; Gardner et al. 2000), and it provides us with valuable information for the distant universe. On the other hand, deep surveys in the near infrared (NIR) wavelengths such as the  $K$  band are also very im-

portant because the uncertainties in the evolutionary effect of galaxies and extinction by dust are less significant for galaxies observed in the NIR than in optical.

One of the deepest images in the NIR has been obtained recently by the 8.2m Subaru telescope: the Subaru Deep Field (SDF, Maihara et al. 2001). The field of view is  $2' \times 2'$  with the total integration time of 12 hours for the  $J$  band and 10 hours for the  $K'$  bands, with the average seeing of about 0.4 arcsec. The 5-sigma limiting magnitude is  $K=23.5$  (in total magnitude), and 350 objects are detected down to this magnitude. In this paper we report a detailed comparison of the counts, colors, and size

distributions of the faint galaxies observed in the SDF with a standard theoretical model of galaxy formation and evolution, to obtain implications for overall galaxy evolution on the cosmological scale.

A number of observational studies on the faint galaxy number counts in the  $K$  band have been published (e.g., Mobasher et al. 1986; Gardner et al. 1993; Glazebrook et al. 1994; McLeod et al. 1995; Djorgovski et al. 1995; Gardner et al. 1996; Moustakas et al. 1997; Huang et al. 1997; Bershadsky et al. 1998; Minezaki et al. 1998, Szokoly, et al. 1998; Saracco et al. 1999; Väisänen et al. 2000), and compilation of these counts are shown in Fig. 1. However the present status of the faint-end  $K$  counts is rather controversial. Indeed, the counts of Bershadsky et al. (1998) are larger by a factor of more than 3 than those of Moustakas et al. (1997) at  $K \sim 23$ , as shown in Fig. 1.

One of the possible origins of this discrepancy is the systematic uncertainty in deriving the observational galaxy counts<sup>1</sup>. Generally the detection of galaxies at the faintest magnitudes is not complete and the completeness depends heavily on the detection criterion, seeing, and galaxy size, surface brightness, and luminosity profile (either exponential or de Vaucouleurs' law). The published faint NIR counts are generally corrected for incompleteness of detection probability, but the procedure of the incompleteness correction is different from one author to another, and model-dependent. This systematic uncertainty is especially significant for high-redshift galaxies at the faintest magnitudes, because there is a well-known physical selection effect against high-redshift galaxies: the geometrical effect of the expanding universe makes the surface brightness of galaxies rapidly dimmer with increasing redshift as  $S \propto (d_A/d_L)^2 \propto (1+z)^{-4}$ , where  $d_A$  and  $d_L$  are the angular diameter distance and luminosity distance, respectively. In fact, Totani & Yoshii (2000, hereafter TY00) has shown that this effect of the cosmological dimming is significant for the HDF galaxies.

The scheme to estimate photometric magnitude, such as aperture, isophotal, or corrected total magnitudes, is also important. The isophotal magnitude measures only the photons within the detection isophote determined by the threshold surface brightness of galaxy detection, and this scheme tends to underestimate the flux of the faintest galaxies near the detection limit. On the other hand, aperture magnitude tends to underestimate the flux of brightest objects when a fixed aperture is adopted. The low counts of Saracco et al. (1999) at  $K \lesssim 20$  may be due to this effect. The total magnitude is generally model-dependent, and one must be careful in a comparison between the counts as a function of corrected total magnitude and general theoretical prediction.

The above consideration suggests that there is an inconsistency in comparing theoretical models with published counts already corrected in a model-dependent way. Therefore, the best way to derive implications on galaxy formation and cosmology is that observed raw data are compared *consistently* with realistic theoretical predictions which take into account the completeness and selection effects under the observational conditions (Yoshii 1993; Yoshii & Peterson 1995; TY00). The primary purpose of this paper is to perform such analyses and derive the most reliable results from the faint NIR galaxies in the SDF.

Generally there are many parameters and systematic uncertainties in the theoretical prediction of galaxy counts, and this has also been one of the origins of the controversy in this field.

In this paper we present a comprehensive survey of systematic uncertainties in the model used here, by which the readers can check how our results could be affected by model uncertainties. We try to make our conclusions unbiased as far as possible after careful examination of such uncertainties.

The paper will be organized as follows. The theoretical model of galaxy formation and evolution used in this paper is described in §2. The procedure to compare the model and SDF data taking into account the selection effects and completeness is described in §3 in detail. The results of comparison of various models versus observed counts, colors and size distributions are given in §4. The summary of this paper will be given in §5.

## 2. THEORETICAL MODEL

The theoretical model used here is based on the present-day properties of galaxies and their observed luminosity function (LF), and it probes the evolution backward in time (Tinsley 1980; Yoshii & Takahara 1988; Fukugita et al. 1990; Rocca-Volmerange & Guiderdoni 1990; Yoshii & Peterson 1991, 1995; Pozzetti et al. 1996, 1998). We use the same model as that used in TY00 to analyze the HDF galaxies, and here we summarize important properties of the model. Galaxies are classified into five morphological types of E/S0, Sab, Sbc, Scd, and Sdm, and their evolution of luminosity and spectral energy distributions (SEDs) is described by a standard galaxy evolution model in which the star formation history is determined to reproduce the present-day colors and chemical properties of galaxies (Arimoto & Yoshii 1987; Arimoto, Yoshii, & Takahara 1992). We will also try a similar but independent evolution model by Kobayashi, Tsujimoto, & Nomoto (2000) based on a different stellar population database (Kodama & Arimoto 1997), to see a typical uncertainty concerning stellar population synthesis models. Type mix is determined by the type-dependent present-day LF as described below. All galaxies are simply assumed to be formed at a single redshift,  $z_F$ , and the sensitivity of our conclusion to this uncertain parameter will be checked by changing this parameter in a range of  $z_F = 3-10$ .

The number density of galaxies is normalized at  $z = 0$  by the  $B$ -band local LF of galaxies, and  $B$ -band magnitude is translated into any band of interest by using the colors of model galaxies which are dependent on galaxy types. This treatment makes it possible to predict multiband galaxy counts with a consistent normalization. Therefore the local  $K$ -band LF is an output of our model, and it will be compared with the observations of the local  $K$ -band LF. We use several published  $B$ -band LFs (the SSRS2 survey, Marzke et al. 1998; the APM survey, Loveday et al. 1992; the CfA survey, Huchra et al. 1983) which are either type-dependent or type-independent. It should be noted that we will try considerably different morphological type mixes by this treatment, and hence we can estimate the sensitivity of the model prediction to the adopted morphological type mix, as well as to the LF. Their Schechter parameters are tabulated in Table 1 of TY00. In all these LFs, the E/S0 galaxies, whose relative proportion is more significant in the NIR than in the optical, is treated as a single population. However, in this paper we will find that the model with such LFs does not fit well to the faintest  $K$  counts, and we will investigate a LF in which the giant and dwarf elliptical galaxies are treated as distinct populations. This treatment is motivated by local observations for giant and dwarf elliptical galaxies in groups and clusters of galaxies (see §4.1.3).

<sup>1</sup> Relatively higher counts by Väisänen et al. (2000) may be due to clusters of galaxies in their field, as discussed by Väisänen et al.

We should examine whether our model is consistent with the local  $K$ -band luminosity function, because the normalization of galaxy number density of our model is set by the  $B$ -band luminosity function as mentioned above. This can be done easily by translating the  $B$ -band luminosity function used in TY00 by the colors of model galaxies at  $z = 0$  which is dependent on the galaxy types. Figure 2 shows the comparison of the model  $K$ -band LF obtained in such a way with the observed  $K$ -band luminosity function in the literature. The figure shows that our model is well consistent with the  $K$ -band LF data, and there is no problem in the normalization of galaxy number density at  $z = 0$ , although the normalization is set by the  $B$ -band LF rather than the  $K$  band.

Absorptions by interstellar dust and intergalactic HI clouds are taken into account. The dust opacity is assumed to be proportional to the gas column density and metallicity, and we adopt two models of spatial distribution of dust such as the intervening screen model and the slab (i.e., the same distribution for stars and dust) model. The observed correlation between the power-law index of UV spectra and the Balmer line ratio of starburst galaxies indicates that the observed reddening of starburst galaxies is larger than expected from the slab model, and at least some fraction of dust should behave like a screen (Calzetti, Kinney, & Storchi-Bergmann 1994). We then use the screen model as a standard, and use the slab model to check the uncertainties. Finally, we use the optical depth calculated by Yoshii & Peterson (1994) for intergalactic absorption by HI clouds. However, the absorption of intergalactic HI clouds is almost negligible at the  $K$  band for galaxies with  $z_F \lesssim 10$ .

The size and surface brightness profile of galaxies are very important for the detectability of faint galaxies, and it must be modeled when the selection effects are taken into consideration. The exponential and de Vaucouleurs' law are assumed for the surface brightness profiles of spiral and elliptical galaxies, respectively. We then assume that the effective radius,  $r_e$ , which is the scale in the exponents, is independent of observed wavelength. We use the relation between the  $B$ -band luminosity and  $r_e$  estimated by fitting to observed  $B$ -band luminosity profile of local galaxies, to calculate  $r_e$  as a function of the present-day  $B$ -band luminosity. It should be noted that, although the effective radius is the same, the observed size of high- $z$  or faint galaxies can be considerably different in different observation bands, because of different sensitivities for surface brightness. Indeed, these effects (the so-called morphological  $k$ -correction) are taken into account in our analysis (see the next section). The relation of the present  $B$  luminosity  $L_B$  and effective radius  $r_e$  is assumed to be a power-law as  $r_e \propto L_B^{2.5/p}$  for each galaxy type, and the normalization and  $p$  are determined by fits to the empirical relation observed for local galaxies. There is a considerable scatter in the empirical  $r_e$ - $L_B$  relation (about 0.22 in  $\log r_e$ ), and the systematic uncertainty due to this scatter will be checked (see TY00 and §4.1.1). In most of our calculations (except in §4.3), we assume that the size evolution of galaxies occurs only when there is number evolution of galaxies. The size evolution which may happen even when there is no merging of galaxies, which we call 'intrinsic' size evolution, will be tested in §4.3.

There may be systematic biases in the estimate of effective radius by the  $B$ -band luminosity profile. One possible origin of bias is dust extinction. The dust opacity is larger in the central region of galaxies, and then the optical scale length, which is more severely affected by extinction, tends to be larger than that estimated by the near-infrared luminosity profile. For

elliptical galaxies, Pahre, de Carvalho, & Djorgovski (1998) found  $\langle \log r_{e,K} \rangle - \langle \log r_{e,V} \rangle = -0.08$ . Difference of  $r_e$  between  $B$  and  $V$  bands can be inferred from the mean color gradient  $d(B-V)/d \log r_e$  (Sparks & Jørgensen 1993), and then we obtain  $\langle \log r_{e,K} \rangle - \langle \log r_{e,B} \rangle = -0.10$ . For spiral galaxies, the difference in  $r_e$  is found as  $\langle \log r_{e,K} \rangle - \langle \log r_{e,B} \rangle = -0.09$  (for face-on spiral galaxies, de Jong 1996) and  $\langle \log r_{e,K} \rangle - \langle \log r_{e,B} \rangle = -0.19$  (for edge-on spiral galaxies, de Grijs 1998). These biases are within the range of the scatter in  $r_e$ - $L_B$  relation mentioned above, and hence the systematic uncertainty in galaxy counts by these biases is also checked in §4.1.1.

A simple picture for galaxy evolution is a so-called pure luminosity evolution (PLE) model in which there is no number evolution of galaxies to high redshifts (Tinsley 1980; Yoshii & Takahara 1988; Fukugita et al. 1990; Rocca-Volmerange & Guiderdoni 1990; Yoshii & Peterson 1991, 1995; Pozzetti et al. 1996, 1998). However, some number evolution is naturally expected in the hierarchically clustering universe dominated by cold dark matter, which is the standard theory of structure formation (e.g., Blumenthal et al. 1984; Kauffmann, White, Guiderdoni 1993; Cole et al. 1994). In order to investigate the possible number evolution of galaxies we introduce a simple merger model characterized by the evolution of the Schechter parameters of LFs, in which the total luminosity density is conserved, i.e.,  $\phi^* \propto (1+z)^\eta$  and  $L^* \propto (1+z)^{-\eta}$  (Rocca-Volmerange & Guiderdoni 1990; Yoshii 1993). For the simplicity, we assume that all types of galaxies have the same number evolution. Indeed, later in this paper (§4.1.2) we will find that this seems not the case in reality. This model is clearly a simplified picture of galaxy merging ignoring the possible starbursts induced by mergers, and this point should be kept in mind in the following analysis. The size evolution induced by the number evolution is modeled by a parameter  $\xi$ , in which the characteristic luminosity and size of individual galaxies satisfy a scaling relation  $L \propto r^\xi$  during the merger process. If the surface brightness or stellar luminosity density within a galaxy is not changed in mergers, this parameter becomes  $\xi = 2$  or 3, respectively. Conversion of merging kinetic energy into random stellar motions would make  $\xi$  smaller, while dissipation of gas would have an inverse effect. We assume  $\xi = 3$  in this paper as a reference value, but the prediction of galaxy counts is actually almost insensitive to  $\xi$  in a reasonable range of  $\xi \sim 2-4$ , unless extremely strong number evolution ( $\eta \gtrsim 5$ ) is invoked. (TY00).

### 3. COMPARING THE OBSERVATIONS AND MODELS

Here we describe in detail the procedure used to compare the observed data in the SDF and the theoretical model. The systematic selection effects taken into account are as follows: (1) apparent size and surface brightness profiles of galaxies where the cosmological dimming is taken into account, (2) dimming of an image by seeing, (3) detection criteria of galaxies under the observational conditions of SDF, (4) completeness of galaxy detection, and (5) photometric scheme and its measurement error. In this paper we use isophotal magnitudes consistently for the data and the theoretical model, unless otherwise stated, to avoid uncertainties in extending the photometry beyond the detection isophote.

#### 3.1. Detection Criteria of SDF

The detection criteria of the SDF is briefly summarized below. See Maihara et al. (2000) for the observations and detail of data reduction. The reduced SDF frames are first smoothed

out by a Gaussian filter with the image resolution of  $0''.55$  in FWHM. Then the detection thresholds are defined at the  $1.50\sigma$  level of surface brightness fluctuation in the sky, which corresponds to the threshold surface brightness (detection isophote) of  $S_{\text{th}} = 25.59$  mag arcsec $^{-2}$  in the  $J$  band and  $24.10$  mag arcsec $^{-2}$  in the  $K'$  band. Objects with isophotal area of 18 pixels ( $A_{\text{th}} = 0.24$  arcsec $^2$ ) or more above the detection isophote are registered as sources detected. Therefore, the faintest isophotal magnitude of objects detected by the SDF is  $K'_{\text{lim}} = 25.65$ . For reference, we plot the total and isophotal  $K'$  magnitudes estimated by Maihara et al. (2000) in Fig. 3, for galaxies detected not only in the  $K'$  band but also in the  $J$  band, to remove spurious noise objects. This plot shows that our analysis will probe galaxies with total magnitudes of  $K' \lesssim 24.5$ , which corresponds to  $\sim 2$  sigma level.

Since we have modeled the galaxy size and the profile of surface brightness profiles, we can calculate the isophotal area and isophotal magnitude of a given galaxy at arbitrary redshift, by using  $S_{\text{th}}$  of SDF. Therefore the above detection criteria can be incorporated in the theoretical prediction of raw galaxy counts. The cosmological dimming of surface brightness and morphological  $k$ -corrections are included here. See TY00 for technical details.

### 3.2. Raw Counts with Isophotal $K$ Magnitudes

Now we present the raw galaxy counts observed in the SDF as a function of isophotal  $K'$  magnitude, which will be compared with theoretical prediction taking into account selection effects. Table 1 shows the number of detected objects ( $N_{\text{det}}$ ), the number of noise objects estimated by the mean of noise frames ( $N_{\text{noise}}$ ), the expected number of detected galaxies ( $N_{\text{gal}} = N_{\text{det}} - N_{\text{noise}}$ ), the galaxy counts  $dN/dm$  [mag/deg $^2$ ] estimated from  $N_{\text{gal}}$ , and its error estimated by  $(N_{\text{det}})^{1/2}$ . In this paper we translate the  $K'$  magnitudes into  $K$  by the formula  $K = K' - 0.1$  based on the typical colors of SDF galaxies. This translation generally depends on colors of galaxies as  $K = K' - 0.056(J - K)$ , but dispersion of  $(J - K)$  color is less than 2 (see Fig. 15), and hence ignoring the color dependence would generate systematic error of at most 0.1 mag, which hardly affects the analysis in this paper. In addition, the magnitude referred here and throughout the paper is not the AB magnitude, but the conventional  $K$  magnitude (e.g., Johnson 1966).

Here we discuss the effect of angular correlation of galaxies which could lead to the systematic uncertainty in the count estimates. Considering an angular area of  $\Omega$ , with a mean count of  $\langle N \rangle$  galaxies, the variance of number of detected galaxies is increased to

$$\mu_2 = \langle N \rangle + \frac{\langle N \rangle^2}{\Omega^2} \int \int \omega(\theta_{12}) d\Omega_1 d\Omega_2, \quad (1)$$

where  $\omega(\theta)$  is the angular correlation function of galaxies and  $\theta_{12}$  is the angle between the points  $d\Omega_1$  and  $d\Omega_2$ . The angular correlation function for faint galaxies has been measured in the  $K$  band by a number of papers (e.g., Baugh et al. 1996; Carlberg et al. 1997; Roche et al. 1999), and it is described in a form of  $\omega(\theta) = A\theta^{-0.8}$ . The amplitude  $A$  at fixed  $\theta$  is a decreasing function of  $K$  magnitude, while there is some evidence that the amplitude becomes relatively flat at  $K \gtrsim 20$  with a value of  $A \sim 1.1 \times 10^{-3}$  when  $\theta$  is measured in degree (Roche et al. 1999). Here we assume the amplitude-magnitude relation does not turn over at  $K \gtrsim 20$ , which is theoretically reasonable (e.g., Roche & Eales 1999), to set the upper limit

on the uncertainty of galaxy counts coming from clustering of galaxies. For the  $1.97' \times 1.9'$  area of the SDF, the variance becomes  $\langle N \rangle + 32.4A\langle N \rangle^2$ . The number of detected SDF galaxies per each magnitude bin of Table 1 is larger than  $\gtrsim 30$  at  $K \gtrsim 21$  and, with the above value of  $A$ , the standard deviation for  $\langle N \rangle = 30$  is  $\sigma = \mu_2^{1/2} = (30 + 32.1)^{1/2}$ . In Table 2, we show the combined error coming from Poisson statistics and clustering, at representative three magnitudes of  $K = 21.25, 23.25$ , and  $24.75$ , along with other model uncertainties which will be discussed later in detail.

### 3.3. Detection Probability of Galaxies (Completeness)

Because of the noise and statistical fluctuations, the source detection is not complete even if true magnitude and size of a source meet the criteria described in the previous section. The  $K'$  band detection completeness of SDF estimated by simulations is shown as a function of total magnitude, for a source having a Gaussian profile with several values of FWHM by solid lines in Fig. 4. The incompleteness is caused by the fluctuation of isophotal area by noise, that often leads to the observed isophotal area smaller than the threshold isophotal area, even if the true isophotal area is larger than the threshold.

We model this incompleteness as follows, in the theoretical prediction of raw galaxy counts. We found that the dispersion of observed isophotal area from the true value can be fitted by the following empirical formula:

$$\sigma_A(m, d_{\text{ob}}) = c(A_1 - A_2)^{1/2} d_{\text{ob}}, \quad (2)$$

where  $m$  and  $d_{\text{ob}}$  are the total magnitude and FWHM size of an object, and  $A_1$  and  $A_2$  the isophotal area corresponding to the isophotal level 0.8 and 1.2 times brighter than  $S_{\text{th}}$ , respectively. The proportionality constant  $c$  is determined to reproduce the result of simulations. Assuming a Gaussian distribution of observed isophotal area with the above dispersion, we can calculate the probability that the observed isophotal area is larger than the threshold value  $A_{\text{th}}$ . We plotted this probability in Fig. 4 by dashed lines, and this result shows that the above empirical formula gives a reasonable estimate of the completeness.

For each model galaxy, we calculate the isophotal size and isophotal magnitude, and then the detection probability from the above formula. Then galaxies are counted considering the detection probability, to derive the raw theoretical galaxy counts which should be compared with raw SDF counts. The practical method to calculate the isophotal area of the image of a model galaxy with given redshift and isophotal magnitude, after Gaussian smoothing ( $0''.55$  in FWHM for SDF) of either an exponential or de Vaucouleurs's profile, has been given in TY00.

### 3.4. Effect of Error in Magnitude Estimate

The photometric error in the estimate of magnitudes in the faint end may be significant, and may modify the slope of  $N$ - $m$  relation. Here we correct the galaxy counts for this effect as follows. Let  $m_{\text{noise},1}$  be the  $1\sigma$  noise level for photometric measurement of an image with area of 1 arcsec $^2$ . For the  $K'$  band observation of the SDF,  $m_{\text{noise},1} = 25.53$ . Then the error for the isophotal magnitude of an image with isophotal area  $A$  (in units of arcsec $^2$ ) is given by  $m_{\text{noise}} = m_{\text{noise},1} - 1.25 \log A$ . Let  $N_0(m_0)$  be the raw galaxy counts per unit isophotal magnitude at  $m_0$  without taking into account the photometric error, which has been calculated by the procedure described in the previous sections. We can also calculate the average completeness  $C_{\text{av}}(m_0)$

and average isophotal area  $A_{\text{av}}(m_0)$  (in arcsec<sup>2</sup>) of galaxies as a function of  $m_0$  from a specified model of galaxy evolution. Then the observed counts  $N_{\text{obs}}(m_{\text{obs}})$  can be calculated as

$$N_{\text{obs}}(m_{\text{obs}}) = \int dm_0 N_0(m_0) P(m_{\text{obs}}; m_0), \quad (3)$$

where  $P(m_{\text{obs}}; m_0)$  is the probability distribution of  $m_{\text{obs}}$  for a galaxy with the true magnitude  $m_0$ . A reasonable form of this probability is

$$P(m_{\text{obs}}; m_0) = \frac{G[m_{\text{obs}}; m_0, \sigma(m_0)] C_{\text{av}}(m_{\text{obs}})}{\int dm_{\text{obs}} G[m_{\text{obs}}; m_0, \sigma(m_0)] C_{\text{av}}(m_{\text{obs}})}, \quad (4)$$

where  $G(x; x_{\text{av}}, \sigma)$  is the Gaussian distribution with an average  $x_{\text{av}}$  and the standard deviation  $\sigma$ . It should be noted that this distribution is weighted by completeness  $C_{\text{av}}(m_{\text{obs}})$ , to account for the fact that a galaxy with brighter  $m_{\text{obs}}$  can be more efficiently detected than that with fainter  $m_{\text{obs}}$ , even if  $m_0$  is the same. Finally, the dispersion  $\sigma(m_0)$  can be written as

$$\sigma(m_0) = 2.5 \log\{1 + 10^{0.4(m_0 - m_{\text{noise},1})} [A_{\text{av}}(m_0)]^{1/2}\}. \quad (5)$$

In fact, we found that this correction for the photometric error is almost negligible (less than a few percent in counts), and the uncertainty of this correction hardly affects the conclusions derived in this paper.

Now we can calculate the observed raw counts  $N_{\text{obs}}(m_{\text{obs}})$  in which all the observational selection effects mentioned above are taken into account using a realistic model of galaxy evolution, and we will compare the counts as well as size and color distributions with the SDF data in the following of this paper.

## 4. RESULTS

### 4.1. Galaxy Counts

Figure 5 shows the prediction of our standard pure luminosity-evolution (PLE) model in a  $\Lambda$ -dominated flat universe [ $(h, \Omega_0, \Omega_\Lambda) = (0.7, 0.2, 0.8)$ ] with screen type dust,  $z_F = 5$ , and the SSRS2 LF, showing the contribution of each morphological type of galaxies to the total counts. It is evident from this figure that elliptical galaxies are the dominant component at  $K \lesssim 20$ , while the contribution by spiral galaxies increases at fainter magnitudes. This is rather insensitive to the model employed here, because it is a consequence of red colors of elliptical galaxies observed in the local universe. For convenience, we take this model as a standard in the following of this paper.

As mentioned above, the raw SDF counts are shown as a function of isophotal magnitude and all the observational selection effects are taken into account in the theoretical curves that should be compared with the raw SDF counts. We did not plot other deep  $K$  counts at  $K > 20$  because it is not possible to interpret them on the same ground as the SDF counts obtained under different observational conditions and completeness corrections. Only the other counts brighter than  $K = 20$  are shown as a function of total magnitude to fix the normalization of the counts. The selection effects under the SDF condition are completely negligible in the bright magnitude range of  $K < 20$ . (See Fig. 6 below).

#### 4.1.1. Sensitivity to Model Parameters

The sensitivity of the prediction to various model parameters should be examined before deriving implications. Here we show how the prediction of galaxy counts changes when the model parameters are changed, using the PLE model in the  $\Lambda$ -dominated universe ( $\Lambda$ -PLE model, shown in Fig. 5) as a standard model. Then we argue that the galaxy count prediction

depends mostly on cosmology and/or number evolution, and other systematic uncertainties are generally smaller than these two.

Figure 6 shows the degree of selection effects incorporated in the theoretical prediction of galaxy counts. For comparison with the standard  $\Lambda$ -PLE model in which the selection effects are taken into account (solid line), the dotted line shows the true galaxy counts as a function of total magnitude without any observational selection effects. The luminosity-size relation observed for local galaxies has considerable scatter for which we have adopted a single power-law fit to calculate the selection effects, and the uncertainty arising from this scatter must be checked. The dashed and dot-dashed lines show the predictions by shifting the luminosity-size relation by  $+1$  and  $-1\sigma$  dispersion in the direction of  $\log r_e$ , respectively. (See Fig. 3 of TY00 for the luminosity-size relation used here.)

Figure 7 shows the dependence on the modeling of galaxy evolution. The solid line is for the standard  $\Lambda$ -PLE model in which the galaxy evolution models of Arimoto & Yoshii (1987) and Arimoto, Yoshii, & Takahara (1992) have been used. The dot-dashed line is for a different galaxy evolution model of Kobayashi, Tsujimoto, & Nomoto (2000). The difference between the solid and dot-dashed lines can then be considered as a typical uncertainty from current models of galaxy evolution based on stellar population synthesis. The dotted line is for an extreme case of assuming no luminosity evolution of galaxies. The dashed line is for the slab model for dust distribution rather than the screen model adopted as the standard, and the difference between the solid and dashed lines corresponds to a typical uncertainty from spatial distribution of dust. Figure 8 shows the sensitivity to the adopted formation redshift  $z_F$  and local luminosity functions of galaxies. As noted earlier, we can also check the sensitivity to the morphological type mix by trying various type-dependent local luminosity functions.

Then Figure 9 shows the theoretical predictions for three representative cosmological models: a low-density flat universe with the cosmological constant (solid), a low-density open universe (dashed), and the Einstein-de Sitter universe (dot-dashed), with  $(h, \Omega_0, \Omega_\Lambda) = (0.7, 0.2, 0.8)$ ,  $(0.6, 0.2, 0.0)$ , and  $(0.5, 1, 0)$ , respectively. The prediction for the standard model, but for the cases of number evolution with  $\eta = 1$  and 2 is shown in Fig. 10.

The summary of these results are tabulated in Table 2, showing the change in galaxy number counts by the change of various model parameters, cosmology, and number evolution. We conclude from these results that the prediction of galaxy counts depends mostly on cosmology and number evolution with  $\eta \gtrsim 1$ . The total systematic uncertainty in count prediction except for cosmology and number evolution is smaller than the difference between  $\Lambda$  and open universes, and less than one third of the difference between  $\Lambda$  and EdS universes. Although our survey of model uncertainties may not be perfect, it does not seem so easy to change the count prediction as large as the effect of cosmological models or number evolution by choosing different values for other parameters in galaxy evolution.

#### 4.1.2. Implications for Cosmology and Merger History of Galaxies

The low-density,  $\Lambda$ -dominated flat universe is currently the most favored from various observational constraints, such as the fluctuation of the cosmic microwave background radiation (de Bernardis et al. 2000) or high- $z$  Type Ia supernova data (Riess

et al. 1998; Perlmutter et al. 1999). Although some systematic uncertainties may still remain in these results (see, e.g., Aguirre 1999; Totani & Kobayashi 1999), the  $\Lambda$ -dominated flat universe is becoming a standard cosmological model. In fact, TY00 has performed the first comprehensive comparison between HDF galaxies and realistic theoretical models taking into account various selection effects, and shown that the galaxy counts and photometric redshift distributions in the HDF are simultaneously reproduced best in the  $\Lambda$ -dominated flat universe. The PLE model in an open universe or the Einstein-de Sitter (EdS) universe underpredicts the observed counts, and even a strong number evolution, if invoked to match the observed counts in a way that luminosity density is conserved, is still seriously inconsistent with the slope of optical counts ( $B_{450}$  and  $V_{606}$ ) and photometric redshift distributions. A similar result has recently been obtained by He et al. (2000).

Then we discuss here implications of the SDF counts assuming this popular  $\Lambda$ -dominated flat universe. In this universe, the observed SDF counts are in reasonable agreement with the PLE model prediction at  $K \lesssim 22.5$ . This indicates that there is almost no room for a number evolution of galaxies with  $\eta \gtrsim 1$ , otherwise the galaxy counts would be seriously overproduced as shown in Fig. 10. This constraint especially applies to relatively giant galaxies with  $\sim L^*$ , since the flattening of the  $N-m$  slope beyond  $K \sim 19$ , where this constraint is obtained, is caused by  $L^*$  galaxies at  $z \sim 1$ . It is in sharp contrast to the case of HDF counts which rather favor a modest number evolution with  $\eta \sim 1$  (TY00). This discrepancy may come from a clearly too simple assumption in the modeling of the number evolution, i.e., the same number evolution for all types of galaxies. We suggest that this apparent discrepancy is due to type-dependent number evolution of galaxies, because the dominant population consists of late-type galaxies in the optical bands whereas early-type galaxies in the near-infrared bands. Therefore, the optical HDF and near-infrared SDF data could be consistently explained if there is some number evolution in late-type galaxies, while almost no number evolution in early-type or elliptical galaxies. To verify this hypothesis, we plot the model predictions where early type galaxies (E/S0 and/or Sab) have no number evolution, while other types have number evolution with  $\eta \sim 1$ , in Fig. 11. As shown in the figure, number evolution of galaxies later than Sbc hardly changes the count prediction in the  $K$  band from the PLE model for all types.

On the other hand, it is also worth considering what degree of number evolution is necessary to match other cosmological models to the data. Figure 12 is the same as Figure 10, but for the case of the EdS universe. A number evolution driven by mergers with  $\phi^* \propto (1+z)^\eta$  can reconcile the observed  $K$  counts and the EdS universe, provided  $\eta \sim 2$ . We also found that this number evolution model is consistent also with the  $(J-K)$ -color and size distributions which will be discussed in the next section, and hence the SDF data alone cannot discriminate between the PLE model in the  $\Lambda$ -dominated universe and the number evolution model in the EdS universe. However, as described above, the  $\Lambda$ -dominated universe is now becoming a standard cosmological model. In fact, TY00 has shown that a strong number evolution of  $\eta \gtrsim 4$  is required to match the EdS universe with the HDF counts. Such a strong number evolution does not seem to be favored by observations. Le Fèvre et al. (2000) argued that typical  $L^*$  galaxies have experienced about 1 major merger from  $z = 1$  to 0, from the HST images of the

Canada-France Redshift Survey (CFRS) galaxies. This corresponds to  $\eta \sim 1$  which is consistent with the result of TY00, and disfavors too large  $\eta$ . We will consider the  $\Lambda$ -PLE model as the standard in the following of this paper.

#### 4.1.3. Evidence for Giant-Dwarf Transition of Elliptical Galaxies

Here we discuss some possible interpretations of the excess of  $K$  counts beyond that predicted by the  $\Lambda$ -PLE model at  $K \gtrsim 22.5$ . A simple interpretation for this is number evolution which cannot simply be expressed by the phenomenological form used in this paper. The number evolution investigated in this paper assumes the same number evolution in all luminosity range, and such evolution would overproduce the relatively bright counts at  $K \lesssim 23$ , even if it may fit to the faintest counts of  $K \gtrsim 23$ , as shown by Fig. 10. A possible scenario is then that number evolution is especially stronger for dwarf galaxies with no or weaker number evolution for giant early-type galaxies, in order not to violate the counts at  $K \lesssim 23$ .

But here we give another possibility, in which an evidence for dwarf elliptical galaxies observed at the local universe gives a natural explanation for the excess. In the above PLE model the elliptical galaxies are treated as a single population having a single LF. However, it is known that the present-day giant elliptical galaxies with  $M_B \lesssim -17$  and dwarf elliptical galaxies with  $M_B \gtrsim -17$  are distinct populations showing different luminosity profiles (the  $r^{1/4}$  law for giants, while exponential for dwarfs) and different luminosity-size relations (see, e.g., Ferguson & Binggeli 1994 for a review). In the  $K$ -band, this critical magnitude corresponds to  $M_K \sim -21$  from the typical color of elliptical galaxies (see Fig. 2). Since the contribution of early-type galaxies is more significant in the near-infrared than in the optical, it is important to take into account such distinct populations of elliptical galaxies in predicting the  $K$  counts in the SDF.

We then model the giant and dwarf elliptical galaxies separately. It is known that the present-day LF of giant elliptical galaxies is well described by a Gaussian-like shape rather than the Schechter function, while the LF of dwarf elliptical galaxies can be fitted by the Schechter function with  $\alpha \sim -1.3$  (e.g., Ferguson & Sandage 1991; Thompson & Gregory 1993). The normalizations of these two populations are roughly the same in poor groups, while the ratio  $\phi_{\text{dwarf}}^*/\phi_{\text{giant}}^*$  seems to increase monotonically with the richness of galaxy groups up to the rich clusters. Here, following Chiba & Yoshii (1999), we adopt the LFs of these two populations with  $M_B^* \sim -19.7$  for giants and  $-16.7$  for dwarfs ( $h = 1$ ). The normalization of  $\phi^* \sim 3.2 \times 10^{-3} h^3$  is used in common for both giants and dwarfs, while a factor  $\exp(-10^{0.4(M-M_{\text{cut}})})$  with  $M_{\text{cut}} = -17.0$  is multiplied to the faint end of giants' LF to match their observed Gaussian-like LF. The SSRS2 LF is used for spiral galaxies. The  $K$ -band LF predicted by this modeling is shown in Fig. 2. This LF is again consistent with the observed  $K$ -band LF, and difference from the other LF models can be seen only in the faint end of  $M_K \gtrsim -20$ . Thus, this model of LF should be considered as one of possible LFs within the observational constraints. The uncertainty of the present-day LF has the most significant effect in the faintest magnitudes of galaxy counts.

The evidence of the two distinct populations can be seen in Fig. 13, where the luminosity-size relation of local elliptical/spheroidal galaxies is shown. We use the fits shown by the

solid and dashed lines as the luminosity-size relations of giants and dwarfs, respectively. The de Vaucouleurs' law ( $r^{1/4}$  law) is adopted as the surface brightness profile for giants while the exponential law for dwarfs, as observed. Finally, the galaxy evolution model of Arimoto & Yoshii (1987) with smaller mass of  $10^{10}M_{\odot}$  is used for dwarfs, while the  $10^{12}M_{\odot}$  model for giants which is the same as that used in the previous sections where elliptical galaxies have been treated as a single population.

Figure 14 shows the prediction of  $K$  counts by the  $\Lambda$ -PLE model with distinct giant and dwarf elliptical populations described above. As can be seen, the transition of giant and dwarf elliptical galaxies occurs at  $K \sim 21$ – $22$ , which corresponds to  $M_K \sim -21$  at the local universe. This two-population model is in excellent agreement with the observed counts over the entire range of  $K$  magnitude. Therefore, the excess of the observed counts at  $K \gtrsim 22.5$  beyond the PLE-model prediction with a single elliptical population can naturally be interpreted as the emergence of a distinct population of dwarf elliptical galaxies that have been observed in the local universe. The count around  $K \sim 20$  is also better reproduced by this model, than the previous model whose counts were systematically higher than the SDF data. In that case number evolution is not necessary to explain the faintest SDF counts. It is difficult to discriminate the two interpretations (i.e., number evolution or distinct elliptical populations) from the current data because of the uncertainty in the faint-end slope of the present-day LF. In the rest of this paper, we use this two-population model in the  $\Lambda$ -dominated universe as the standard.

#### 4.2. $(J-K)$ -Color Distribution

Figure 15 shows the observed  $(J-K)$ -color distribution for the SDF galaxies (crosses) which are detected in both the  $J$  and  $K$  bands with the magnitudes measured in  $1''.156$  aperture, which has been used as the aperture to measure aperture magnitude of SDF galaxies. (Here we use aperture magnitude because the definition of isophotal magnitude depends on the threshold surface brightness, and hence on different sensitivities of different bands.) The observed mean colors are also shown by filled squares. Theoretical predictions from the standard  $\Lambda$ -PLE model used in Fig. 14 are made with the selection effects taken into account, for the mean color of all galaxy types as well as for individual types.

The prediction for the average of all types (thick solid line) is in reasonable agreement with the observed mean (filled squares). This color-magnitude diagram is not sensitive to cosmology or number evolution with ( $\eta \lesssim 2$ ); the merger model ( $\eta = 2$ ) in the EdS universe is also well consistent with the data, as mentioned earlier. This color-magnitude diagram is more sensitive to the luminosity and color evolution of galaxies, and the prediction under the assumption of no evolution model (thick dashed line) exhibits the largest difference from the standard model. The no evolution model does not fit the data, and this indicates that a current method of stellar population synthesis gives reasonable color evolution of galaxies.

#### 4.3. Size Distributions

Figure 16 shows the observed size distribution for the SDF galaxies (crosses) in terms of isophotal area. The filled squares show the mean of the observed sizes. Theoretical predictions from the standard  $\Lambda$ -PLE model used in Fig. 14 are made under the assumption of no size evolution, for the mean of all galaxy types as well as individual galaxy types. We found a reason-

able agreement between the model (thick solid line) and the observed mean (filled squares). Size evolution which is caused by number evolution does not change drastically the size versus  $K$ -magnitude relation, because both the size and luminosity decrease into high- $z$  by number evolution. Especially, if the typical surface brightness does not change by merger, merging of galaxies hardly affects this plot.

The essential factor in this comparison is then possible 'intrinsic' size evolution which is not caused by number evolution, but which changes the size of galaxies without changing their total luminosity. We here introduce a phenomenological parameter  $\zeta$ , and multiply an additional factor  $(1+z)^{\zeta}$  to  $r_e$  obtained by the modeling described in §2 in which this intrinsic size evolution was not taken into account. Figure 17 shows the  $\Lambda$ -PLE model with various values of  $\zeta$ . (Note that the standard  $\Lambda$ -PLE model used in Fig. 14 is for  $\zeta = 0$ .) Evidently the intrinsic size evolution of galaxies is well constrained by  $-1 \lesssim \zeta \lesssim 0$ , and there is no strong evidence for intrinsic size evolution of galaxies.

#### 4.4. Redshift Distributions

Since neither spectroscopic nor photometric redshifts are yet available for the SDF galaxies, it is instructive to predict the redshift distribution from the models which explain all the existing data such as counts, colors, and sizes of the SDF galaxies. Figure 18 shows the predictions for isophotal  $K$  magnitudes of 20, 22, and 24. The solid and dot-dashed lines are for the standard  $\Lambda$ -PLE model and the EdS merger ( $\eta = 2$ ) model, respectively, where the selection effects are taken into account. Giant and dwarf elliptical galaxies are treated as distinct populations in both of the models.

As can be seen by the figure, the theoretically expected redshift extends to  $z \sim 1$ – $2$ , and the implications obtained by this paper, such as the constraint on the number evolution in the  $\Lambda$ -dominated universe, should apply galaxies in this redshift range. As expected, the redshift distribution from the EdS merger model has a peak at lower redshifts when compared with the standard  $\Lambda$ -PLE model. This difference, though not sufficiently large, may be used to discriminate between the two models.

The dashed line is the redshift distribution from the standard  $\Lambda$ -PLE model, which is the same as shown by the solid line, but for total  $K$  magnitudes with the selection effects not taken into account in the model. It should be noted that the selection effects are only weakly dependent on redshift, in contrast to the case of the HDF, as demonstrated in TY00 and in the analysis of extragalactic background light by Totani et al. (2001). The difference from the HDF is due to the fact that image sizes of the SDF galaxies are about 5 times larger than the HDF galaxies. When the surface brightness is made fainter by larger image size, this non-cosmological dimming becomes dominant compared with the cosmological surface brightness dimming, and the redshift dependence of the selection effects should become weaker. In other words, the cosmological dimming is especially serious when a good sensitivity is achieved by good image resolution rather than large telescope diameter as in the case of the HST.

## 5. DISCUSSION AND CONCLUSION

In this paper we presented a detailed study for the comparison between the near-infrared galaxy counts, colors, and size distributions observed in the Subaru Deep Field (SDF) which

is one of the deepest NIR images of the universe, and theoretical models probing galaxy formation/evolution backward in time based on the present-day properties and number density of galaxies observed at  $z = 0$ . We have paid special attention in taking into account various selection effects consistently in the models, to avoid systematic biases which may have been a possible origin of controversial previous results. The selection effects considered here are (1) apparent size and surface brightness profiles of galaxies where the cosmological dimming is taken into account, (2) dimming of an image by seeing, (3) detection criteria of galaxies under the observational conditions of SDF, (4) completeness of galaxy detection estimated by simulations of SDF, and (5) photometric scheme and its measurement error. (The isophotal or aperture magnitudes are used in a self-consistent way.) The selection effects are found to be negligible at  $K \lesssim 21$  in the conditions of the SDF, and the conclusion in this paper is not affected by uncertainty coming from these effects down to this magnitude limit. Careful treatment of the selection effects described above enabled us to investigate much fainter galaxies down to isophotal  $K = 25.66$  or total  $K \sim 24.5$ . In addition, it is statistically unlikely that the angular clustering of galaxies affects the following results.

We also examined as far as possible the systematic uncertainties in the galaxy evolution models used here, and have shown that the galaxy count prediction mostly depends on cosmology and number evolution, and other examined dependence on model parameters or uncertainties are smaller than the two. Therefore, though our survey of systematic uncertainties may not be perfect, we consider that it is not easy to change the conclusions derived below by choosing other model parameters of galaxy evolution or taking into account the uncertainties.

We have found that the conventional pure-luminosity-evolution model (PLE) in a  $\Lambda$ -dominated flat universe ( $\Lambda$ -PLE model) is well consistent with the observed SDF counts, color, and size distributions down to isophotal  $K \sim 22.5$ , without any signature of number evolution ( $\eta \ll 1$ ), where the number evolution is parametrized as  $\phi^* \propto (1+z)^\eta$  and  $L^* \propto (1+z)^{-\eta}$  for all types of galaxies. On the other hand, a number evolution of  $\eta \sim 2$  is necessary to explain the data in the Einstein-de Sitter universe.

The  $\Lambda$ -dominated universe is now favored by various cosmological observations, and here we discuss several implications from our results, assuming that this universe is the true model. There is almost no room for number evolution of  $L^*$  galaxies with  $\eta \gtrsim 1$  in this universe, otherwise it would overproduce the galaxy counts of  $20 \lesssim K \lesssim 23$ . This result provides a strong constraint on the number evolution of giant elliptical or early-type galaxies with  $L \sim L^*$  which are expected to be a dominant population at  $K \lesssim 20-23$ . Since their expected redshift distribution extends to  $z \sim 1-2$ , we conclude that there is no evidence for the number evolution of giant elliptical galaxies to  $z \sim 1-2$ , which is consistent with other observational constraints by different approaches (Totani & Yoshii 1998; Im et al. 1999; Schade et al. 1999; Benitez et al. 1999; Broadhurst & Bouwens 2000; Daddi, Cimatti, & Renzini 2000). On the other hand, it should be noted that the SDF data do not strongly constrain the number evolution of late type galaxies which are not the dominant population in the NIR bands. The SDF data also suggest a possibility of some number evolution of dwarf galaxies. We have already found some evidence for number evolution of galaxies observed in the optical bands in the Hubble Deep Field (HDF) (TY00). Since late-type spiral galaxies become a

dominant population at optical wavelengths, such a discrepant view of number evolution from the near-infrared SDF and optical HDF data likely reflects the type-dependence of merger history of galaxies, i.e., stronger number evolution for later type galaxies. These conclusions place interesting constraints on the merger history of galaxies in the framework of hierarchically clustering scenario in the CDM universe (e.g., Blumenthal et al. 1984; Kauffmann, White, & Guiderdoni 1993; Cole et al. 1994).

Recently Phillipps et al. (2000) analyzed the number counts of E/S0 galaxies which are selected thanks to the good resolution of HST, and they derived a considerably different conclusion from ours: the EdS universe with simple passive evolution gives an excellent fit to the E/S0 counts. The origin of this discrepancy with our study is not clear, but here we mention several possible origins. First, morphological selection of galaxies sometimes leads to serious systematic bias especially when it is used to study number evolution of a selected galaxy type. Galaxies may have different morphology when observed at different wavelength (i.e., morphological  $k$ -correction), and there may also be physical transition of morphological type. Even if elliptical galaxies have formed at high redshift and then evolved passively, morphology of a galaxy which is observed as an elliptical galaxy at  $z = 0$  may not be recognized as an elliptical galaxy at high redshifts because younger stellar population still exists at young age of the galaxy and it may not reach dynamical relaxation. Such possible systematic effect is difficult to check, but could lead to systematic bias when we study number evolution or cosmology by number counts of a selected galaxy type. Second, it seems that the selection effects against high- $z$  galaxies are not included in Phillipps et al. (2000), and this may have resulted in loss of high- $z$  galaxies extended by the cosmological dimming effect. In fact, the selection effects are already becoming important at  $I_{814} \gtrsim 20$  (see Fig. 6 of TY00). Note that the selection effects against extended sources are more serious in HDF than SDF, because the good sensitivity of HST is achieved by good resolution rather than the telescope diameter. Third, the luminosity evolution is assumed in a simple form of  $L \propto (1+z)^x$  in Phillipps et al. (2000). It may be a good approximation at low redshift, but a clearly too simple modeling at high redshifts. Our model is based on a more realistic luminosity and SED evolution model and especially, it includes dust absorption. As shown by TY00, it is naturally expected that elliptical galaxies at starburst phase are very dusty and hard to detect in optical wavelengths.

We have found a slight excess of observed counts compared with the PLE prediction at  $K \gtrsim 22.5$ , which may be a signature of some number evolution for dwarf galaxies. However we have also shown that this excess can naturally be resolved within the  $\Lambda$ -PLE model, if we treat giant and dwarf elliptical galaxies separately as distinct populations having different luminosity functions and surface brightness profiles, as suggested by observations of elliptical galaxies in local groups and clusters (Ferguson & Binggeli 1994; Ferguson & Sandage 1991; Thompson & Gregory 1993). The faintest counts are sensitive to the faint-end of the local LF which is poorly constrained by observation, and it does not allow us to derive strong conclusions at the faintest magnitudes.

The  $(J-K)$ -color and size distributions of the SDF galaxies are also well explained by both of the two models which can explain the SDF counts, i.e., the PLE model in  $\Lambda$ -dominated flat universe and the merging model ( $\eta \sim 2$ ) in the EdS universe,



and there is no evidence for intrinsic size evolution not caused by number evolution. A no-luminosity-evolution model fails to reproduce the observed color distributions, and this result gives an overall validity to typical luminosity evolution models of galaxies based on stellar population synthesis.

TT and YY acknowledge partial support from Grants-in-Aid for Scientific Research (12047233) and COE Research ((07CE2002) of the Ministry of Education, Science, and Culture of Japan.

#### REFERENCES

- Aguirre, A.N., 1999, *ApJ*, 512, L19  
 Arimoto & Yoshii 1987 *Jari87* Arimoto, N., & Yoshii, Y. 1987, *A&A*, 173, 23  
 Arimoto, Yoshii & Takahara 1992 *Jari92* Arimoto, N., Yoshii, Y., & Takahara, F., 1992, *A&A*, 253, 21  
 Baugh, C.M., Gardner, J.P., Frenk, C.S., & Sharples, R.M. 1996, *MNRAS*, 285, L15  
 Bender, R., Burstein, D. & Faber, S.M. 1992, *ApJ*, 399, 462  
 Benitez, N., Broadhurst, T.J., Bouwens, R.J., Silk, J., & Rosati, P. 1999, *ApJ*, 515, L65  
 Bershad, M.A., Lowenthal, J.D., & Koo, D.C. 1998, *ApJ*, 505, 50  
 Blumenthal, G.R., Faber, S.M., Primack, J.R., & Rees, M.J. 1984, *Nature*, 311, 517  
 Broadhurst, T.J. & Bouwens, R.J., 2000, *ApJ*, 530, L53  
 Calzetti, D., Kinney, A.L., & Storch-Bergmann 1994, *ApJ*, 429, 582  
 Carlberg, R.G., Cowie, L.L., Songaila, A., & Hu, E.M. 1997, *ApJ*, 484, 538  
 Chiba, M. & Yoshii, Y. 1999, *ApJ*, 510, 42  
 Cole, S., Aragon-Salamanca, A., Frenk, C.S., Navarro, J.F., & Zepf, S.E. 1994, *MNRAS*, 271, 781  
 Cole, S. et al. 2001, astro-ph/0012429, to appear in *MNRAS*.  
 Daddi, E., Cimatti, A., & Renzini, A. 2000, *A&A* 362, L45  
 de Bernardis, P. et al. 2000, *Nature*, 404, 955  
 de Grijs, R. 1998, *MNRAS*, 299, 595  
 de Jong, R.S. 1996, *A&A*, 313, 377  
 Djorgovski, S. et al. 1995, *ApJ*, 438, L13  
 Ferguson, H.C. & Binggeli, B. 1994, *A&A Rev.* 6, 67  
 Ferguson, H.C. & Sandage, A. 1991, *AJ*, 101, 765  
 Fukugita, M., Takahara, F., Yamashita, K., & Yoshii, Y. 1990, *ApJ*, 361, L1  
 Gardner, J.P., Cowie, L.L., & Wainscoat, R.J. 1993, *ApJ*, 415, L9  
 Gardner, J.P., Sharples, R.M., Carrasco, B.E., & Frenk, C.S. 1996, *MNRAS* 282, L1  
 Gardner, J.P., Sharples, R.M., Frenk, C.S., & Carrasco, B.E. 1997, *ApJ*, 480, L99  
 Gardner, J.P. et al. 2000, *AJ*, 119, 486  
 Glazebrook, K., Peacock, J.A., Miller, L., Collins, C.A. 1994, *MNRAS*, 266, 65  
 He, P., Zhen-Long, Z., & Yuan-Zhong, Z. 2000, *Ap&SS*, 274, 557  
 Huang, J.-S., Cowie, L.L., Gardner, J.P., Hu, E.M., Songaila, A., and Wainscoat, R.J. 1997, *ApJ*, 476, 12  
 Huchra, J.P., Davis, M., Latham, D. & Tonry, J. 1983, *ApJS*, 52, 89  
 Im, M., Griffiths, R.E., Naim, A., Ratnatunga, K.U., Roche, N., Green, R.F., & Sarajedini, V.L. 1999, *ApJ* 510, 82  
 Johnson, H.L. 1966, *ARA&A*, 4, 193  
 Kauffmann, G., White, S.D.M., & Guiderdoni, B. 1993, *MNRAS*, 264, 201  
 Kobayashi, C., Tsujimoto, T., & Nomoto, K. 2000, *ApJ*, 539, 26  
 Kodama, T. & Arimoto, N. 1997, *A&A*, 320, 41  
 Le Fèvre, O. et al. 2000, *MNRAS*, 311, 565  
 Loveday, J., Peterson, B.A., Efstathiou, G., & Maddox, S.J. 1992, *ApJ*, 390, 338  
 Maihara, T., et al. 2000, *PASJ*, 53, 25.  
 Marzke, R.O., Nicolaci da Costa, L., Pellegrini, P.S., Willmer, C.N.A., & Geller, M.J. 1998, *ApJ*, 503, 617  
 McLeod, B.A., Bernstein, G.M., Rieke, M.J., Tollestrup, E.V., & Fazio, G.G., 1995, *ApJS*, 96, 117  
 Minezaki, T., Kobayashi, Y., Yoshii, Y., & Peterson, B.A. 1998, *ApJ*, 494, 111  
 Mobasher, B., Sharples, R.M., & Ellis, R.S. 1993, *MNRAS*, 263, 560  
 Moustakas, L.A., Davis, M., Graham, J.R., Silk, J., Peterson, B.A., and Yoshii, Y. 1997, *ApJ*, 475, 445  
 Pahre, M.A., de Carvalho, R.R., & Djorgovski, S.G. 1998, *ApJ*, 116, 1606  
 Perlmutter, S. et al. 1999, *ApJ*, 517, 565  
 Phillipps, S. et al. 2000, *MNRAS*, 319, 807  
 Pozzetti, L., Bruzual, G.A., & Zamorani, G. 1996, *MNRAS*, 281, 953  
 Pozzetti, L., Madau, P., Zamorani, G., Ferguson, H.C. & Bruzual, C.A. 1998, *MNRAS* 298, 1133  
 Riess, A.G. et al. 1998, *AJ*, 116, 1009  
 Rocca-Volmerange, B. & Guiderdoni, B. 1990, *MNRAS*, 247, 166  
 Roche, N., & Eales, S. 1999, *MNRAS*, 307, 703  
 Roche, N., Eales, S.A., Hippelein, H., & Willott, C.J. 1999, *MNRAS*, 306, 538  
 Saracco, P., D'Odorico, S., Moorwood, A., Buzzoni, A., Cuby, J.-G., & Lidman, C. 1999, *A&A*, 349, 751  
 Schade, D. et al. 1999, *ApJ*, 525, 31  
 Sparks, W.B. & Jørgensen, I. 1993, *AJ*, 105, 1753  
 Szokoly, G., Subbarao, M., Connolly, A. & Mobasher, B. 1998, *ApJ*, 492, 452  
 Thompson, L.A. & Gregory, S.A. 1993, *AJ* 106, 219  
 Tinsley, B.M. 1980, *Fund. Cosmic Phys.* 5, 287  
 Totani, T. & Kobayashi, C. 1999, *ApJ*, 526, L65  
 Totani, T. & Yoshii, Y. 1998, *ApJ*, 501, L177  
 Totani, T. & Yoshii, Y. 2000, *ApJ*, 540, 81 (TY00)  
 Totani, T., Yoshii, Y., Iwamuro, F., Maihara, T., & Motohara, K. 2001 *ApJ*, 550, L137.  
 Väisänen, P., Tollestrup, E.V., Willner, S.P., & Cohen, M. 2000, *ApJ*, 540, 593  
 Williams, R.T. et al. 1996, *AJ*, 112, 1335  
 Williams, R.T. et al. 2000, *AJ*, 120, 2735  
 Yoshii, Y. 1993, *ApJ*, 403, 552  
 Yoshii, Y. & Peterson, B.A. 1991, *ApJ*, 372, 8  
 Yoshii, Y. & Peterson, B.A. 1994, *ApJ*, 436, 551  
 Yoshii, Y. & Peterson, B.A. 1995, *ApJ*, 444, 15  
 Yoshii, Y. & Takahara, F. 1988, *ApJ*, 326, 1

TABLE 1  
SDF RAW  $K'$  GALAXY COUNTS IN ISOPHOTAL MAGNITUDES

Isophotal $K'$	$N_{\text{det}}$	$N_{\text{noise}}$	$N_{\text{gal}}$	$\log(dN/dm)$	$\log(dN/dm)$ , Error
16.25	1	0	1	1.93E+3	1.93E+3
16.75	0	0	0	0.00E+0	0.00E+0
17.25	3	0	3	5.78E+3	3.34E+3
17.75	3	0	3	5.78E+3	3.34E+3
18.25	4	0	4	7.71E+3	3.85E+3
18.75	5	0	5	9.63E+3	4.31E+3
19.25	6	0	6	1.16E+4	4.72E+3
19.75	11	0	11	2.12E+4	6.39E+3
20.25	15	0	15	2.89E+4	7.46E+3
20.75	19	0	19	3.66E+4	8.40E+3
21.25	27	0	27	5.20E+4	1.00E+4
21.75	32	0	32	6.17E+4	1.09E+4
22.25	41	0	41	7.90E+4	1.23E+4
22.75	44	0	44	8.48E+4	1.28E+4
23.25	55	0	55	1.06E+5	1.43E+4
23.75	58	1.5	56.5	1.09E+5	1.49E+4
24.25	83	24.0	59.0	1.14E+5	1.99E+4
24.75	201	111.5	89.5	1.72E+5	3.41E+4
25.25	206	159.0	47.0	9.06E+4	3.68E+4
25.75	56	40.5	15.5	2.99E+4	1.89E+4

NOTE.— $N_{\text{det}}$ ,  $N_{\text{noise}}$ , and  $N_{\text{gal}}$  are the number of detected objects, expected noise, and galaxies, respectively, in the SDF. The count and its error are in units of  $\text{deg}^{-2}\text{mag}^{-1}$ .

TABLE 2  
SENSITIVITY OF THE PREDICTED  $K$ -BAND  $N$ - $m$  RELATION TO THE CHANGE OF INPUT MODEL PARAMETERS

Change	$\Delta \log N(m_K)^a$			Figure Ref.
	$m_K = 21.25$	$m_K = 23.25$	$m_K = 24.75$	
1. Luminosity Evolution: on $\rightarrow$ off	-0.033	+0.081	+0.156	7
2. Luminosity Evolution Model: AY, AYT $\rightarrow$ KTN <sup>b</sup>	+0.129	+0.109	+0.085	7
3. Dust absorption: screen $\rightarrow$ slab	+0.048	+0.062	+0.088	7
4. Local LF/type-mix: SSRS2 $\rightarrow$ Stromlo-APM/CfA <sup>c</sup>	-0.032/+0.007	-0.086/-0.047	-0.112/-0.122	8
5. Formation epoch: $z_F = 5 \rightarrow 3/10$	-0.134/+0.073	-0.162/+0.097	-0.171/+0.106	8
6. $r_e$ - $L_B$ relation: $+1\sigma/-1\sigma$ in $\Delta(\log r_e)^d$	-0.035/+0.018	-0.094/+0.057	-0.132/+0.086	6
7. Poisson & Clustering	$\pm 0.111$	$\pm 0.092$	$\pm 0.106$	
8. Total systematic uncertainty <sup>e</sup>	$\pm 0.207$	$\pm 0.226$	$\pm 0.266$	
9. Cosmology: $\Lambda \rightarrow$ open/EdS <sup>f</sup>	-0.270/-0.591	-0.289/-0.666	-0.266/-0.689	9
10. Number Evolution <sup>g</sup> : $\eta = 0 \rightarrow 1/2$	+0.229/+0.371	+0.319/+0.588	+0.374/+0.734	10

<sup>a</sup> Raw counts predicted by the model with selection effects, in the isophotal magnitudes

<sup>b</sup> AY: Arimoto & Yoshii (1987), AYT: Arimoto, Yoshii, & Takahara (1992), KTN: Kobayashi, Tsujimoto, & Nomoto (2000).

<sup>c</sup> See Table 1 of Totani & Yoshii (2000) for detail.

<sup>d</sup> See §2 for detail.

<sup>e</sup> Quadratic sum of the rows 2–7. A mean value of the two numbers in the rows 4–6 is used in the sum.

<sup>f</sup>  $\Lambda$ : ( $\Omega_0, \Omega_\Lambda$ ) = (0.2, 0.8), EdS: (1, 0), open: (0.2, 0)

<sup>g</sup> Luminosity-density conserving number evolution with  $\phi^* \propto (1+z)^\eta$  and  $L^* \propto (1+z)^{-\eta}$ .

NOTE.—The prescriptions of a standard model in our analysis include a  $\Lambda$  cosmology, AY-AYT evolution model, the local LF of SSRS2,  $z_F = 5$ , and the screen model of dust absorption.

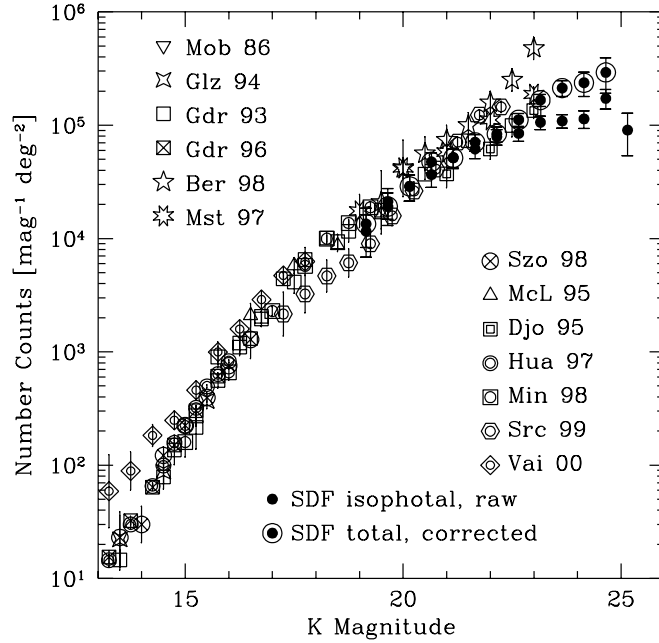


FIG. 1.—  $K$ -band galaxy counts. The data points are Mobasher et al. (1986), Glazebrook et al. (1994), Gardner et al. (1993, 1996), Bershadsky et al. (1998), Moustakas et al. (1997), Szokoly et al. (1998), McLeod et al. (1995), Djorgovski et al. (1995), Huang et al. (1997), Minezaki et al. (1998), Saracco et al. (1999), and Väisänen et al. (2000). The raw counts of the SDF is shown by the filled circles in isophotal magnitudes, while the counts corrected assuming point sources are plotted by the circled dots in total magnitudes (Maihara et al. 2001).

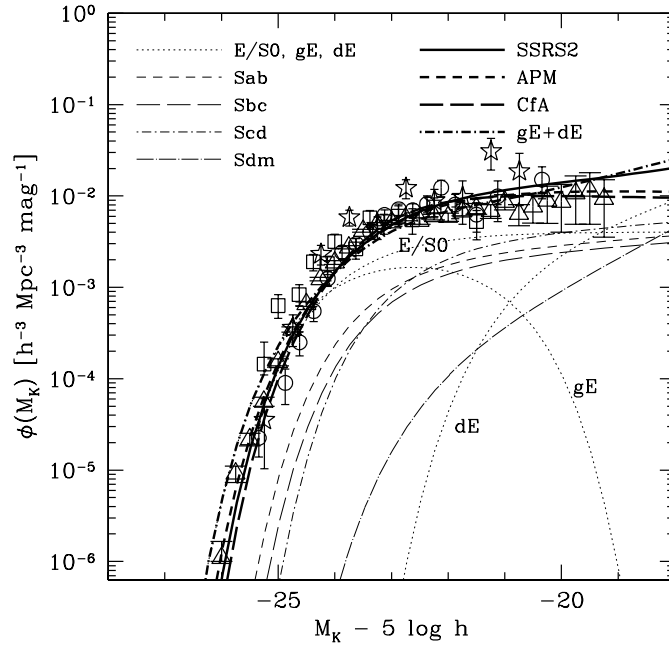


FIG. 2.— Comparison of the theoretical model and observed data of the  $K$ -band luminosity function in the local universe. The thick curves are the model predictions for the total of all galaxy types, which are based on the  $B$ -band LF of SSRS2 (Marzke et al. 1998), APM (Loveday et al. 1992), and CfA surveys (Huchra et al. 1983) (see Table 1 of Totani & Yoshii 2000 for the summary of the Schechter parameters). The thick dot-dashed line is the same as the SSRS2 LF, but two populations of giant and dwarf elliptical galaxies (gE and dE, respectively) are incorporated instead of the single elliptical population of E/S0. (see §4.1.3 for detail.) The thin curves are for individual galaxy types of the SSRS 2 LF, and the types are indicated in the figure. The data points are Mobasher et al. (1993, open squares), Gardner et al. (1997, open circles), Szokoly et al. (1998, stars), and Cole et al. (2001, triangles).

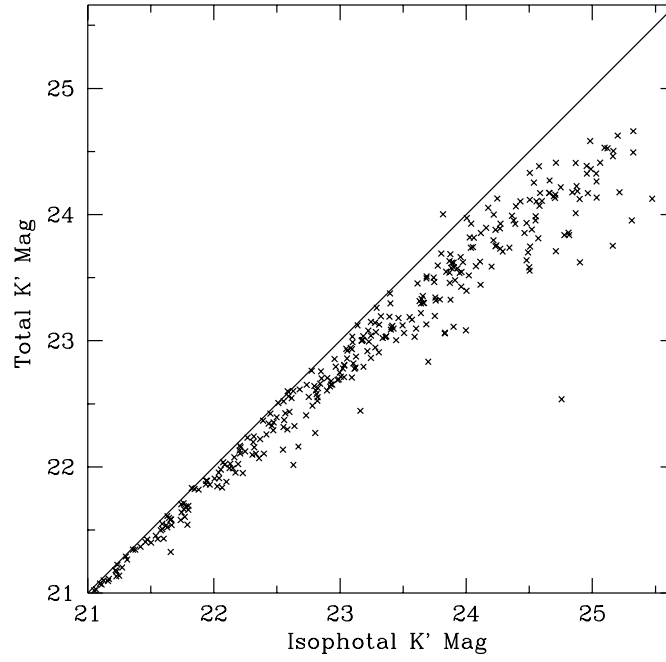


FIG. 3.— The total versus isophotal  $K'$  magnitudes estimated for galaxies detected in both the  $J$  and  $K'$  bands in the Subaru Deep Field (SDF).

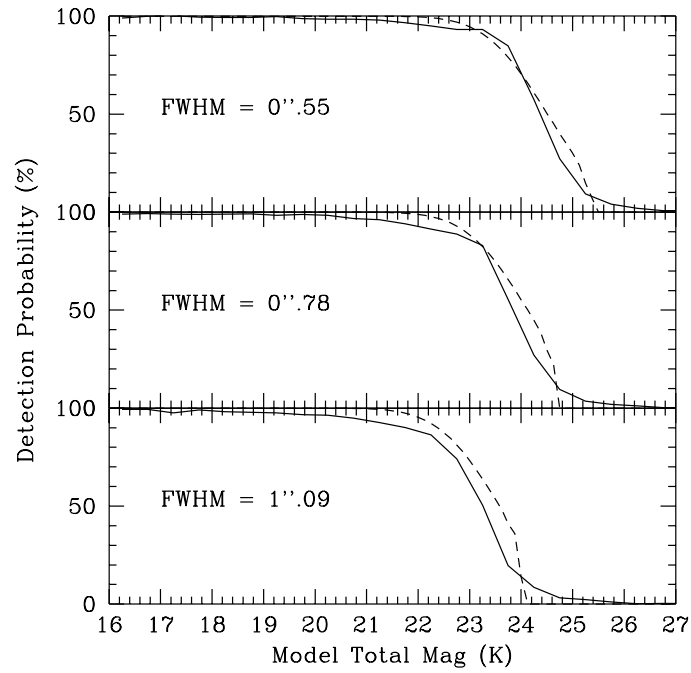


FIG. 4.— Detection probability in the SDF for an object having a Gaussian profile for several values of FWHM. The solid lines are the results of simulations, while the dashed lines are those of the empirical formula used in the theoretical predictions based on the distribution of isophotal area of galaxy images. The image resolution is set to be  $0''.55$  equal to that of the SDF.

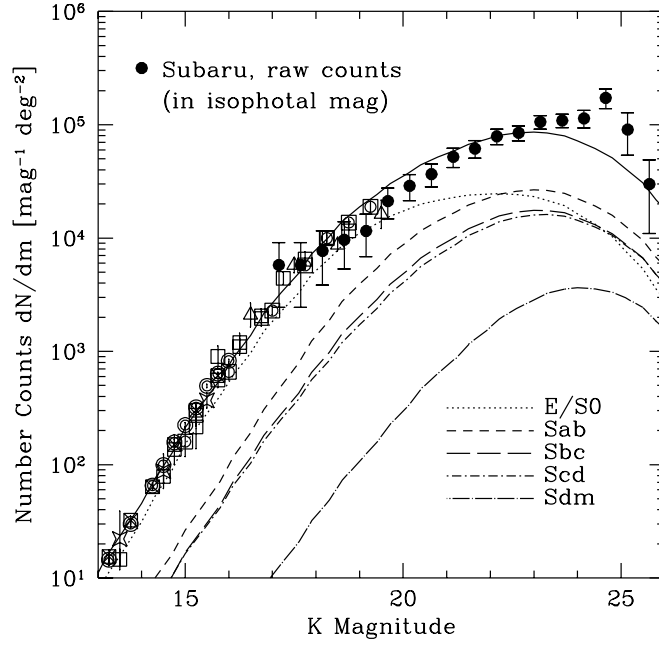


FIG. 5.— Galaxy counts in the  $K$  band. Shown are the  $\Lambda$ -PLE model predictions for individual types of galaxies, in which the selection effects are taken into account and it should be compared with the raw SDF counts in isophotal magnitudes (filled circles). The solid line is for the total of all types of galaxies. The dotted, short-dashed, long-dashed, short-dot-dashed, and long-dot-dashed lines are for E/S0, Sab, Sbc, Scd, and Sdm, respectively. See Figure 1 for the references of the data points. The deep  $K$  counts ( $K > 20$ ) previously published are not plotted in this figure because the detection criteria are different from that of the SDF.

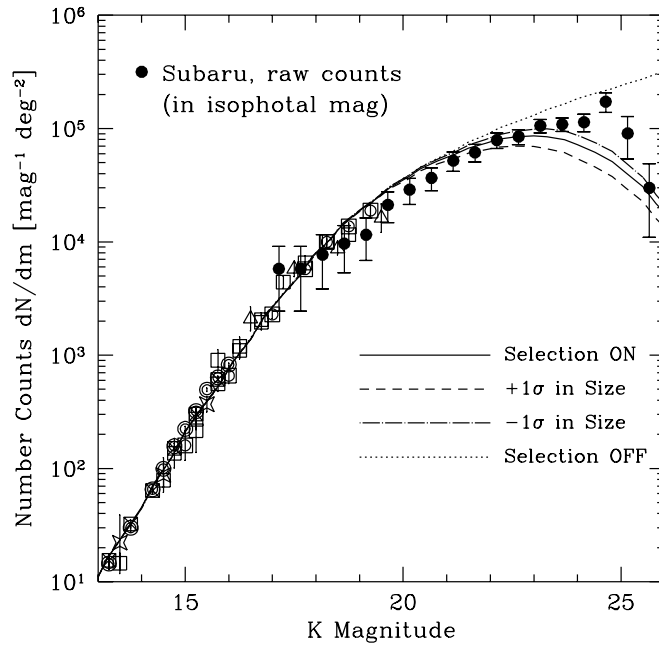


FIG. 6.— Galaxy counts in the  $K$  band. Shown are the  $\Lambda$ -PLE model predictions with and without the selection effects taken into account in the calculations. The solid line is the prediction with the selection effects as a function of isophotal magnitudes, which is same as shown by the solid line in Fig. 5. The dotted line is the prediction without the selection effects, where the number is given as a function of total  $K$  magnitude. The dashed and dot-dashed lines show the predictions from shifting the observed luminosity-size relation of local galaxies by  $+1$  and  $-1\sigma$  dispersion in the direction of effective radius  $\log r_e$ , respectively.

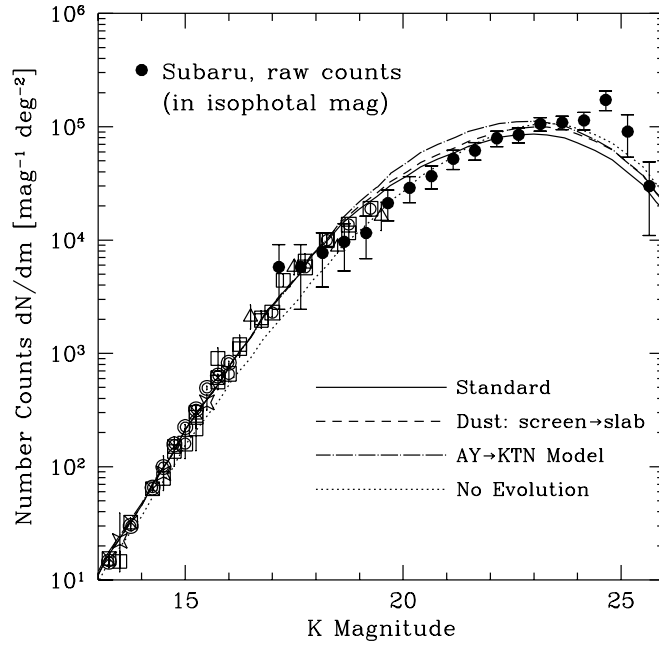


FIG. 7.— Galaxy counts in the  $K$  band. Shown are the  $\Lambda$ -PLE model predictions by changing various model parameters. The solid line is the standard prediction with the Arimoto-Yoshii population-synthesis model of galaxy evolution and the screen model for spatial dust distribution, which is the same as shown by the solid line in Fig. 5. The dotted line is for the no-evolution model of galaxies, and the dot-dashed line is for a different population-synthesis model of galaxy evolution. The dashed line is the prediction with the slab model for spatial dust distribution. (See text for details.)

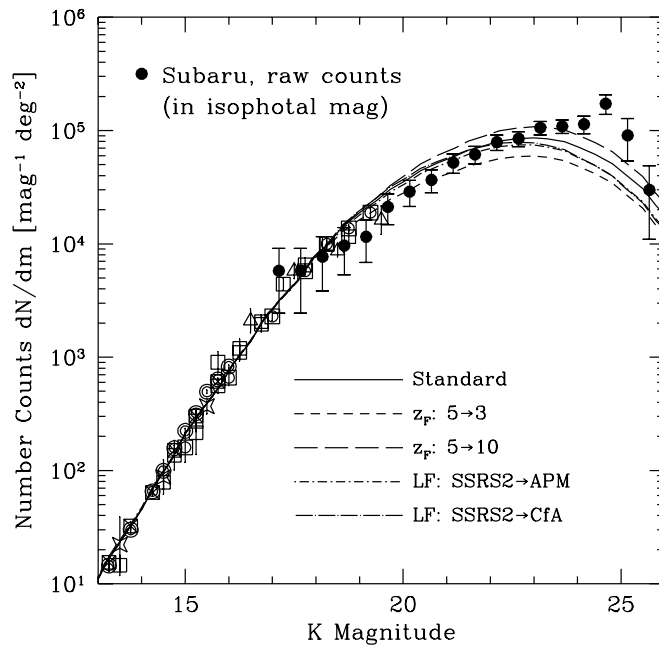


FIG. 8.— Galaxy counts in the  $K$  band. Shown are the  $\Lambda$ -PLE model predictions from changing the formation redshift ( $z_F$ ) and the present-day  $B$ -band luminosity function (LF). The solid line is the standard prediction with  $z_F = 5$  and the LF of the SSRS2 survey, which is the same as shown by the solid line in Fig. 5. The short-dashed and long-dashed lines are the predictions with  $z_F = 3$  and 10, respectively. The short-dot-dashed and long-dot-dashed lines are the predictions with the LF of the APM and CfA surveys, respectively. For the Schechter parameters of these type-dependent LFs, see Table 1 of TY00.

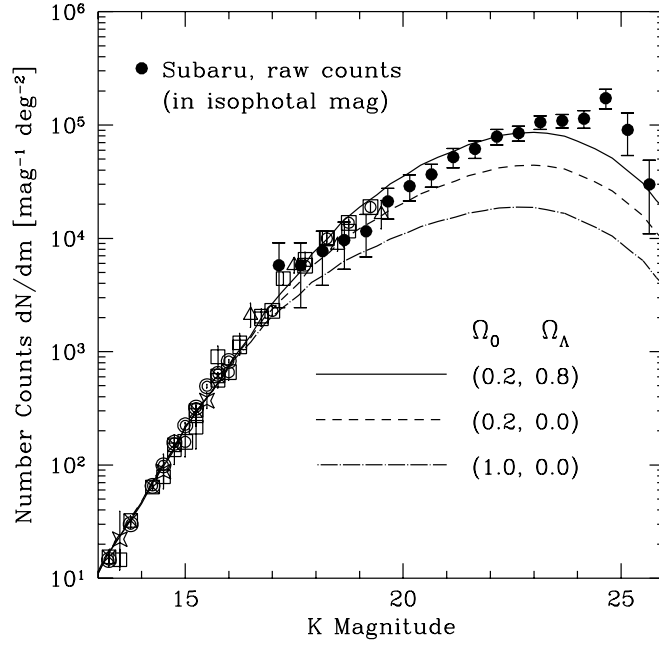


FIG. 9.— Galaxy counts in the  $K$  band. The solid, dashed, and dot-dashed lines are the PLE predictions, for the cosmological models of  $(h, \Omega_0, \Omega_\Lambda) = (0.7, 0.2, 0.8)$ ,  $(0.6, 0.2, 0)$  and  $(0.5, 1, 0)$ , respectively. The solid line is the same with our standard model shown in Fig. 5.

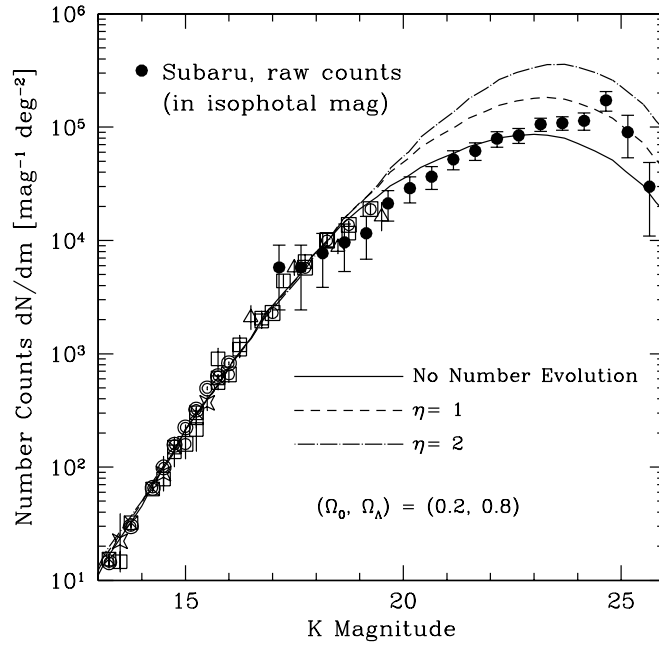


FIG. 10.— Galaxy counts with number evolution in the  $\Lambda$ -dominated flat universe with  $(h, \Omega_0, \Omega_\Lambda) = (0.7, 0.2, 0.8)$ . The solid line is the PLE prediction with no number evolution, which is the same as shown by the solid line in Fig. 5. The dashed and dot-dashed lines are the predictions with number evolution of  $\eta = 1$  and 2, respectively, when the number density of galaxies is assumed to evolve as  $\phi^* \propto (1+z)^\eta$  while the luminosity density  $\phi^* L^*$  is conserved. (See text for details.)

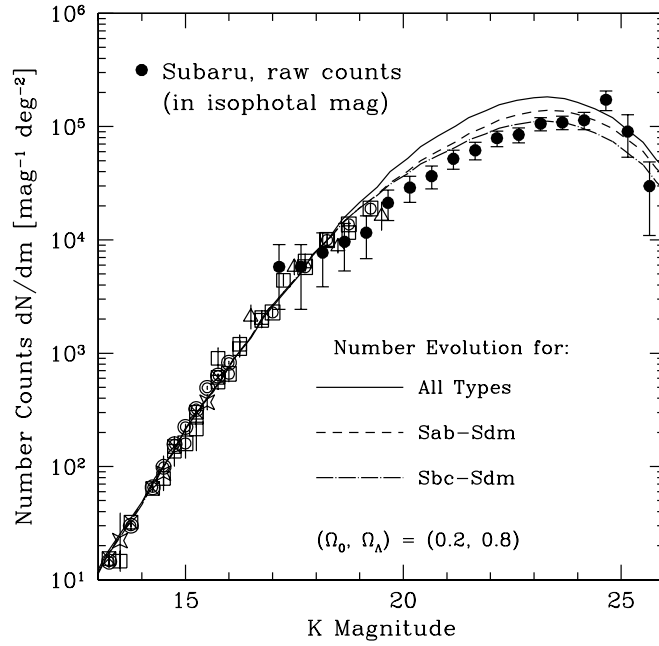


FIG. 11.— Galaxy counts in the  $\Lambda$ -dominated flat universe with  $(h, \Omega_0, \Omega_\Lambda) = (0.7, 0.2, 0.8)$ . The solid line is the prediction with number evolution for all galaxy types ( $\eta = 1$ ), which is the same as shown by the dashed line in Fig. 10. The dashed and dot-dashed lines are the predictions where galaxy types later than Sab and Sbc have number evolution of  $\eta = 1$ , while other types of E/S0 and/or Sab have no number evolution. The dot-dashed line is almost the same with the PLE model for all types. (Our model includes five types of E/S0, Sab, Sbc, Scd, and Sdm, see Fig. 5).

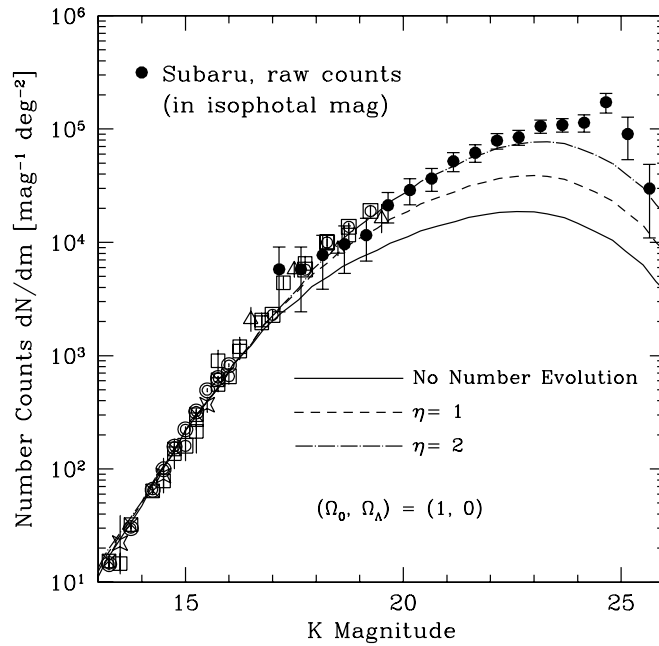


FIG. 12.— Galaxy counts with number evolution in the Einstein-de Sitter universe with  $(h, \Omega_0, \Omega_\Lambda) = (0.5, 1, 0)$ . The solid line is the PLE prediction with no number evolution, which is the same as shown by the dot-dashed line in Fig. 9. The dashed and dot-dashed lines are the predictions with number evolution of  $\eta = 1$  and 2, respectively, when the number density of galaxies is assumed to evolve as  $\phi^* \propto (1+z)^\eta$  while the luminosity density  $\phi^* L^*$  is conserved. (See text for details.)



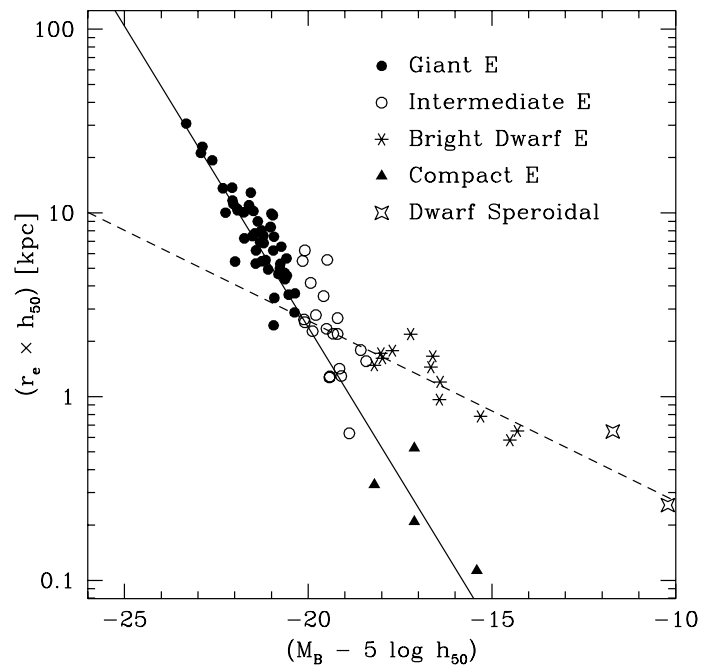


FIG. 13.— Luminosity-size relation of elliptical/spheroidal galaxies observed in the local universe. The data points are from Bender et al. (1992) following their classification into sub-categories. The solid and dashed lines are the fits to the distinct populations of giant and dwarf elliptical galaxies, respectively, which are used to calculate the selection effects in our models.

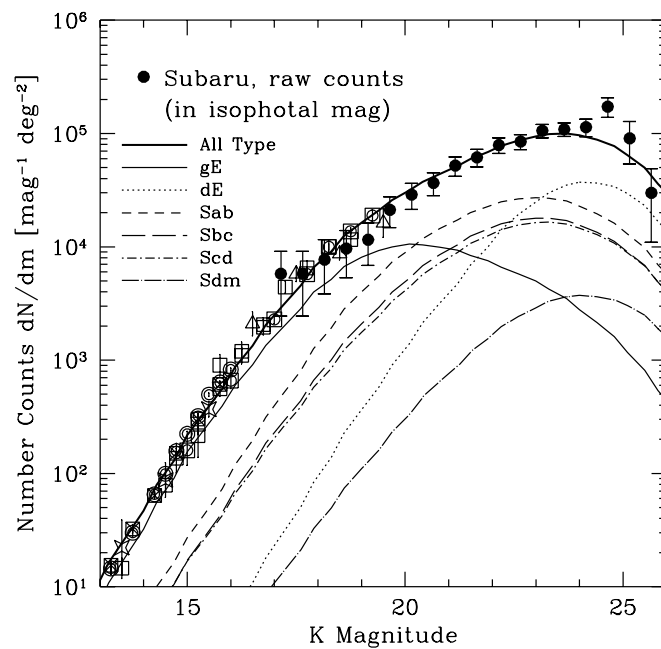


FIG. 14.— Galaxy counts in the  $K$  band in the  $\Lambda$ -PLC model. Same as Fig. 5, but for a model treating the giant and dwarf elliptical galaxies as two distinct populations. The thick solid line is for the total of all types of galaxies, while other six lines are for individual types, as indicated in the figure. The raw SDF counts without employing completeness corrections are shown as a function of isophotal  $K$  magnitude. All known selection effects are included in theoretical calculations to be compared with the raw SDF counts.

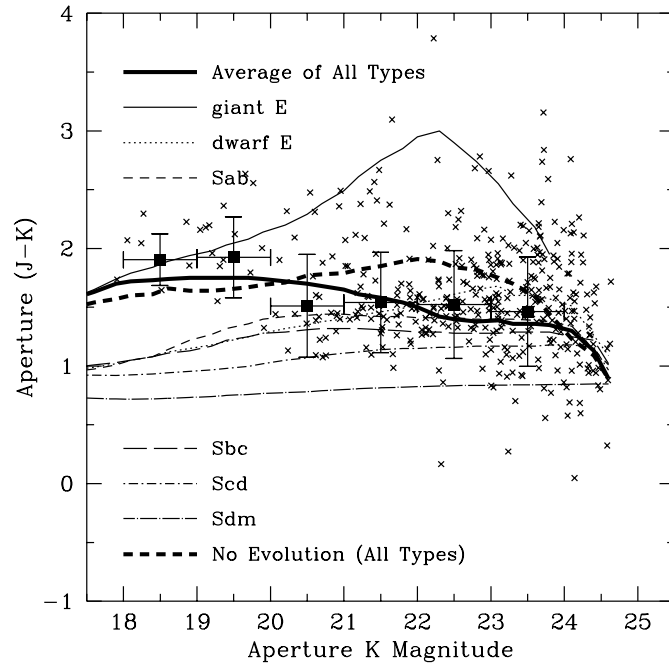


FIG. 15.— Color distribution of the SDF galaxies in the  $(J-K)$  versus  $K$  diagram. The crosses are for individual galaxies, and the filled squares are mean colors within the 1-magnitude intervals shown by the horizontal error bars. The vertical error bars show the  $1\sigma$  dispersion of the colors. Only the SDF galaxies detected in both the  $J$  and  $K$  bands are plotted, and their magnitudes are measured in  $1''.156$  aperture. These detection criteria are consistently taken into account in the theoretical curves. The thick solid line is the predicted mean color for all types of galaxies, based on the  $\Lambda$ -PLE model which is the same as used in Fig. 14. The thin lines are the predictions for individual types of galaxies, and the thick dashed line for the no-evolution model of galaxies.

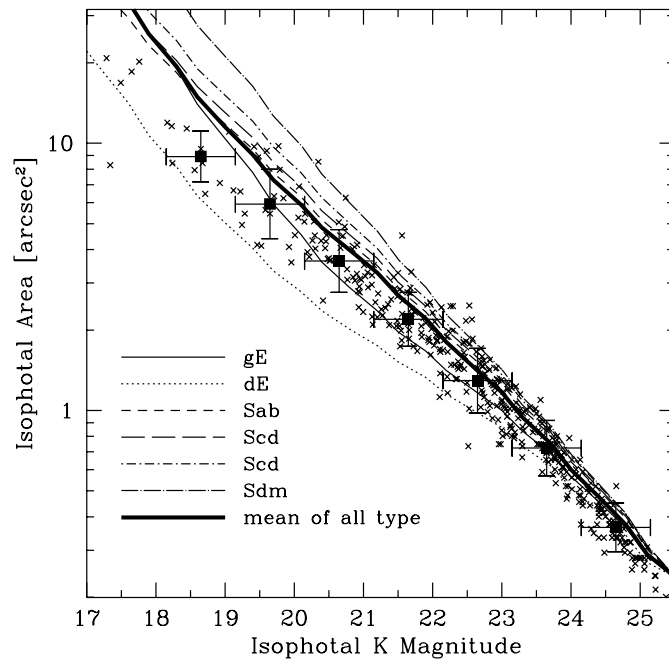


FIG. 16.— Size distribution of the SDF galaxies in the isophotal area versus isophotal- $K$  diagram. The crosses are for individual galaxies, and the filled squares are mean sizes within the 1-magnitude intervals shown by the horizontal error bars. The vertical error bars show the logarithmic  $1\sigma$  dispersion of the sizes. The thick solid line is the predicted mean size for all types of galaxies, based on the  $\Lambda$ -PLE model which is the same as used in Fig. 14. The thin lines are the predictions for individual types of galaxies.

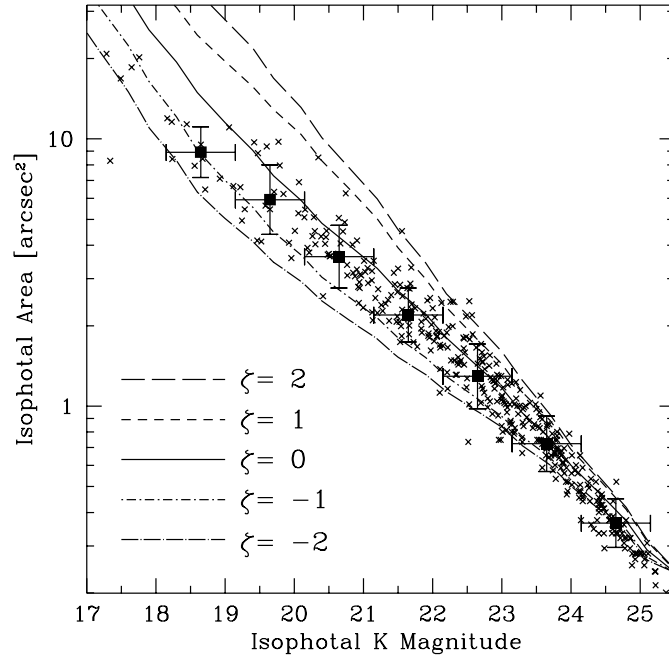


FIG. 17.— Size distribution of the SDF galaxies in the isophotal area versus isophotal- $K$  diagram. Same as Fig. 16, but for allowing intrinsic size evolution of galaxies. The solid line is the predicted mean size for all types of galaxies assuming no intrinsic size evolution, which is identical to the thick solid line in Fig. 16. The short-dashed, long-dashed, dot-short-dashed, and dot-long-dashed lines are the predictions with size evolution of  $\zeta = 1, 2, -1$ , and  $-2$ , respectively, when the effective radius of galaxies is assumed to evolve as  $r_e \propto (1+z)^\zeta$ .

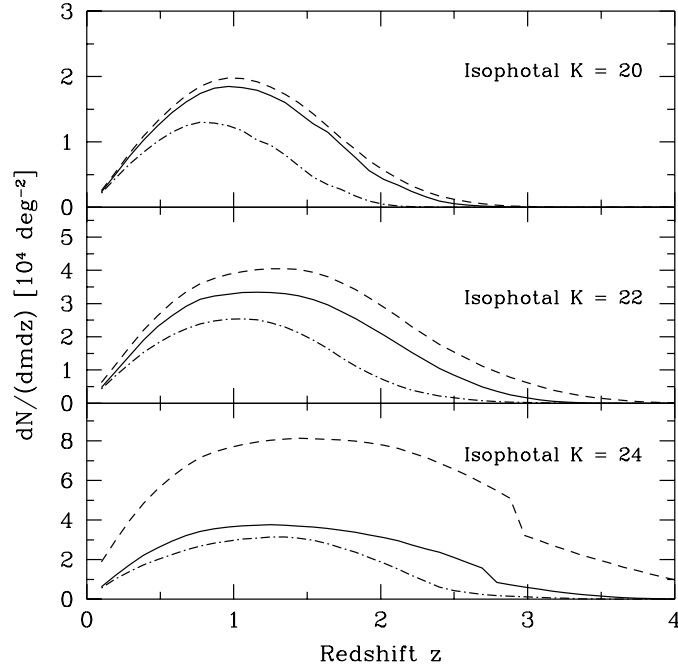


FIG. 18.— Redshift distribution of the SDF galaxies predicted by the models which can explain their observed  $K$  counts,  $(J-K)$ -colors, and isophotal areas. Here all the selection effects are taken into account in theoretical calculations. In each panel showing the predictions for a fixed isophotal  $K$  magnitude, the solid line is the prediction from the  $\Lambda$ -PLC model, which is the same as used in Fig. 14 to calculate the galaxy counts. The dot-dashed line is the prediction from the EdS merger ( $\eta = 2$ ) model, which also fits to the galaxy counts. For only the purpose of comparison with the solid line, the dashed line is shown for the prediction with no selection effects, which highlights the importance of the selection effects in detecting the SDF galaxies.